IEEE Photonics Journal
An IEEE Photonics Society Publication

Open Access

Metasurface-Based Lens for Antenna Gain Enhancement and Radar Cross Section Reduction

Volume 11, Number 6, December 2019

Jianing Yang
Cheng Huang
Jiakun Song
Xu Zhang
Xin Xie
Xiangang Luo

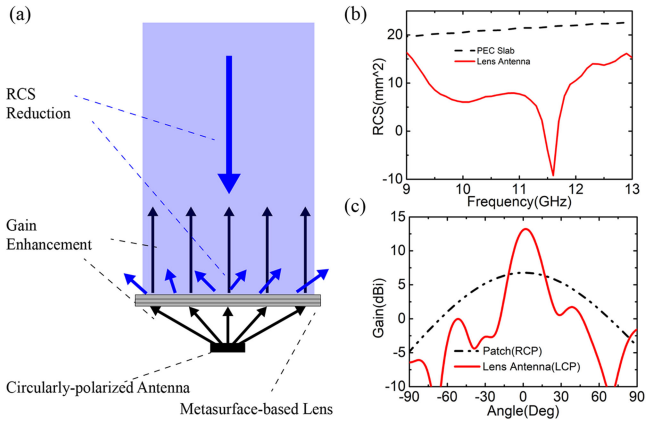

DOI: 10.1109/JPHOT.2019.2950194

Metasurface-Based Lens for Antenna Gain Enhancement and Radar Cross Section Reduction

Jianing Yang,[1,2] Cheng Huang,[1] Jiakun Song,[1] Xu Zhang,[1] Xin Xie,[1,2] and Xiangang Luo [1]

[1]State Key Laboratory of Optical Technologies on Nano-Fabrication and Micro-Engineering, Institute of Optics and Electronics, Chinese Academy of Sciences, Chengdu 610209, China
[2]University of Chinese Academy of Sciences, Beijing 100049, China

DOI:10.1109/JPHOT.2019.2950194

Manuscript received August 7, 2019; revised September 24, 2019; accepted October 24, 2019. Date of publication November 18, 2019; date of current version December 17, 2019. This work was supported in part by the National Natural Science Foundation of China under Grants 61975209 and 61605213, and in part by the Youth Innovation Promotion Association of Chinese Academy of Sciences. Corresponding author: X. Luo (e-mail: lxg@ioe.ac.cn).

Abstract: In this paper, leveraging the resonant phase and the geometry phase simultaneously, we demonstrated a low scattering lens antenna, which can work at both transmission and reflection mode. Different from the traditional microwave lens which only realizes wavefront shaping in half-space, the proposed metasurface lens not only squeezes the transmitted divergent beam to improve the gain of the conventional circular-polarized antenna, but also scatters the electromagnetic wave to maintain a low reflection property in broadband. The proposed lens antenna working in full space may provide a new approach for an integrated communication system.

Index Terms: Lens antenna, low scattering, gain enhancement, metasurface.

1. Introduction

Antenna, as the terminal of the communication systems, plays an irreplaceable role in signal transmitting and receiving. However, it is also a main contributing source to the overall RCS of the communication systems. Thus, reducing the RCS while maintaining the gain of the antenna is crucial to some military communication platform. Traditional methods to reduce the RCS are focusing on the shaping of target surface [1] and applying the absorbing materials. [2] The properly designed geometry shaping can redirect the backward scattering wave to non-threatening direction that the radar cannot receive. The absorbing materials are capable of absorbing the incident wave and converting it to heat. Nevertheless, both the two methods will degrade the radiation performance of the antenna. Hence, some researchers have proposed various low-scattering antennas to eliminate the contradiction between the scattering and radiation, including electromagnetic(EM) band-gap [3]–[5] and frequency selective surface. [6], [7] However, most of them pay less attention to enhancing the radiation performance of the antennas.

A microwave lens is an effective method to enhance the directivity of the antennas. [8] Inspired by the optical lens, the microwave lens is expected to shape the emitting wave from the antenna, leading to gain enhancement of the antennas. Recently, metamaterials-based EM devices have been presented by many researchers. [9]–[11] Metamaterial is an artificial material made of sub-wavelength resonant elements, which can tailor the EM wave as desired. Consequently, some

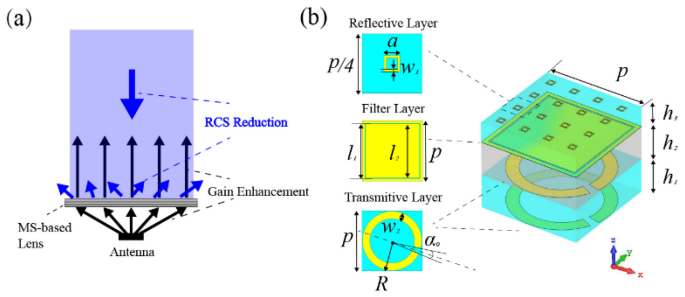

Fig. 1. (a) Schematic model of the proposed metasurface-based lens antenna and (b) unit cell of the lens.

lens antennas emerged, such as the high-directivity antenna based on a gradient refractive index or near-zero-index, [12]–[14] they can morph the incoming wave excited by the primary source to generate the parallel emitting wave. Although the metamaterial-based lens antennas can enhance the radiation performance of the antennas significantly, the bulky size and complex design hinder its further development. As a planer vision of metamaterials, metasurface paves an easier way to manipulate EM wave casually. [15]–[21] So far, several microwave lenses based on have been reported to realize good beam shaping performance by phase compensation. [22]–[30] As expected, these lenses can squeeze the divergent beam excited by the source antenna into a narrow beam, hence improve their radiation performance considerably. Recently, some researchers [31]–[33] have explored to improve the capacity of the microwave lens by introducing bi-functional s. In our previous work, [33] we have experimentally demonstrated a bidirectional beam deflector which can manipulate circular-polarized (CP) transmitted wave and linear-polarized reflected wave simultaneously. Inspired by this design method, we propose a novel metasurface lens to construct a high-gain and low-scattering antenna. The proposed metasurface lens can work in both transmission and reflection modes independently with the aid of a filter layer. In the transmission mode, the phase of transmitted wave excited by the CP antenna can be properly compensated by the metasurface lens, resulting in the enhancement of the antenna directivity. In the reflection mode, we mainly focus on the RCS reduction at X-band since many types of radar are strategically deployed. The metasurface lens can diffuse the back-scattering wave into non-threaten directions through phase cancellation.

2. Design Principle and Unit Cell

Fig. 1(a) shows the schematic model of our metasurface-based lens antenna. The lens is made of the cascaded metasurfaces, which could simultaneously manipulate the transmitted and reflected wavefront. When it is adopted as a superstrate placed in front of an exciting patch antenna, it could be used to not only reshape the EM wave emitted from the patch source into a quasi-plane wave, but also disperse the incoming wave for reducing the backward scattering wave. Therefore, the gain improvement and RCS reduction could be expected. As Fig. 1(b) shows, the meta-atom of this lens is composed of three functional metasurface layers, corresponding to the reflection layer, filtering layer and transmission layer, respectively. The top layer composed of 4×4 square loop array serves as the reflection layer. The period and width of the square loops are set to be $p_1 = p/4 = 3.75$ mm and $w_1 = 0.15$ mm, and the length a would be tuned for obtaining the desired reflection phase coverage. The two layers of the identical split rings at the bottom of the meta-atom operate in the transmitted mode under CP incident wave. By altering the orientations of the split rings, the transmission phase can be continuously tuned based on the Pancharatnam-Berry (PB) phase. [34] The radius R of the split ring is 7.35 mm, and its width w_2 is 1.8 mm, the split angle α_0 is 10°. The middle filtering layer is applied to suppress the cross-talk between the reflection and transmission layers. It is composed of a notch structure with the length of the inner and outer square

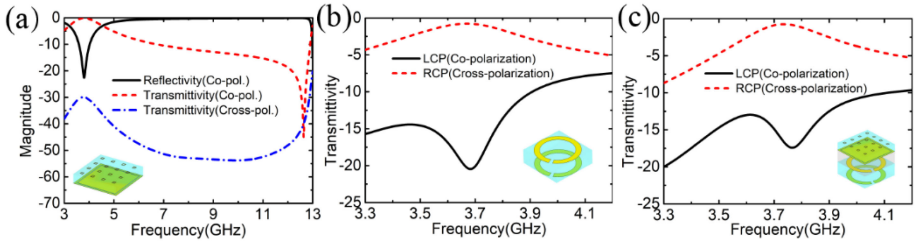

Fig. 2. Reflection and transmission characteristics of the resonant reflected unit cell, the geometry phase unit cell and the cascaded unit cell. (a) The reflection and transmission amplitude of the reflected unit cell in 3–13 GHz. (b, c) The transmission amplitude of the co-polarization and cross-polarization of the geometry phase unit cell in 3.3–4.2 GHz, (b) with and (c) without the filtering layer, in this case, $\beta = 120°$, $a = 2.3$ mm.

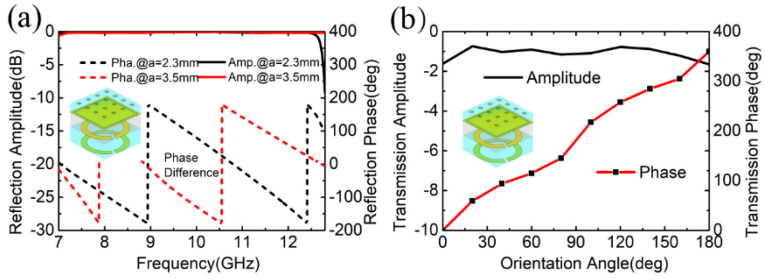

Fig. 3. Reflection and transmission characteristics of the unit cell of the lens. (a) Reflection phase and amplitude of the unit cell under x-polarized wave illumination along the -z direction. The length a of the square loop is respectively, set as 2.3 mm and 3.5 mm, and the orientation angle of β is fixed as 120° for the split ring. (b) Transmission phase and amplitude of the unit cell under an LCP wave along the +z direction (β is varied from 0° to 180° and $a = 2.3$ mm).

patch setting as $l_1 = 13.3$ mm and $l_2 = 13.7$ mm. All the metallic patterns are printed on the F4B (dielectric constant $\varepsilon_r = 2.65$ and loss tangent $\delta = 0.003$) substrates with the thicknesses of $h_1 = 5$ mm and $h_3 = 3$ mm, which is spaced by a foam layer in the middle ($h_2 = 5$ mm).

To characterize the transmission and reflection performance of the proposed unit cell, numerical simulation is performed by using the commercial software CST microwave studio software 2014. In the simulation process, the periodic boundary condition is applied at both x and y directions to emulate the infinite array. Here, the meta-atom of the lens can simultaneously operate in both the transmitted and reflected modes for different frequency bands. The transmitted and reflected frequency bands of interest are respectively set at 3.3–4.2 GHz and 8–13 GHz covering the X-band.

As mentioned above, the meta-atom combines the resonant unit cell and the geometry phase elements together. As seen in Fig. 2(a), the resonant unit cell is composed of the square loops and the backed filtering layer, which reveals a broadband reflection at 8–13 GHz. In the meanwhile, it has a transparent window at about 3.75 GHz to let the EM wave pass through. The geometry phase element is made of two identical split rings, as shown in Fig. 2(b), and it can control the phase of the transmitted EM wave. This transmitted meta-atom works at the transparent window of the reflected layer, and it has a cross-polarized ratio exceeding 10 dB between 3.6 and 3.9 GHz. Consequently, the two distinct single-layer structures are adhered together, and spaced by a foam layer to realize full-space control by using one cascaded metasurface. In Fig. 2(c), the transmission conversion efficiency of the combined meta-atom is not deteriorative compared with the single-layer split ring structure. It is noted that the working band has shifted to high frequency, which is due to the inevitable coupling between the two structures.

Fig. 3 illustrates the simulated reflection and transmission characteristics of the cascaded unit cell. Fig. 3(a) displays the simulated reflection characteristic of the unit cell under the illumination of

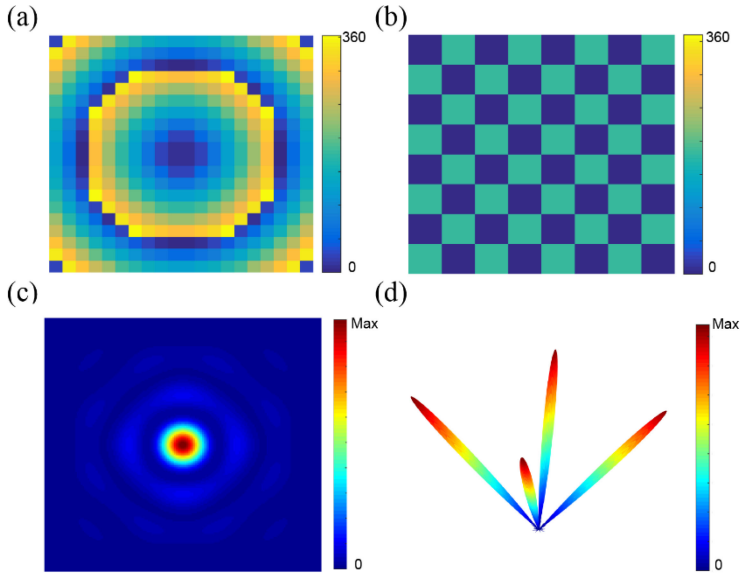

Fig. 4. Phase contributions of the metasurface for transmission (a) and (b) reflection. (c) Calculated transmitted focusing spot at z = 40 mm. (d) Calculated reflected far field pattern.

the x-polarized wave along the −z direction. It is obvious that the two designed loops with different sizes have almost full-reflection properties over the whole band, and the reflection phase difference of 180° ± 37° is obtained in 8.3–12.6 GHz to satisfy the scattering cancellation. [35] Due to the geometric symmetry, the unit cell behaves polarization-insensitive in the reflected mode. For the transmitted mode, the incident left-handed CP (LCP) wave along the +z direction is converted to the right-handed CP (RCP) outgoing wave. As shown in Fig. 3(b), when the orientation angle of β varies from 0° to 180°, the transmission magnitude is kept to be about −1.1 dB in average at 3.75 GHz and the transmission phase tuning range covers the whole 360°, as most of the EM wave passes through and reshaped by the lens.

3. Simulation Results

Based on the proposed unit cell, an metasurface-based lens consisting of 20 × 20 unit cells is constructed to verify its ability to tailor EM waves in both reflection and transmission modes. As seen in Fig. 4(a), in the transmission mode, the phase distribution is designed to focus the EM wave with a focal length of 40 mm. The beam focusing performance is examined by the vector diffraction method as seen in Fig. 4(c), the bright spot at the plane of the focal length proves that transmission phase distribution is able to help the metasurface lens to converge all the outgoing wave energy into the position of $z = 40$ mm. In the reflection mode, we divide the whole reflection into 8 × 8 super unit, and each super unit is a sub-array consisted of 10 × 10 identical square-loop structure. Fig. 4(b) shows the phase distribution that utilizes the 0-180°chess-board configuration. To predict its scattering performance in the far field region, the planar array theory is adopted and the calculated far field pattern is exhibited in Fig. 4(d). It is apparent that the beam is divided into four directions, resulting in a low back-scattering energy [36].

In order to further verify the radiation and scattering performance of the metasurface-based lens antenna, the above full-wave simulation model is designed as shown in Fig. 5. The whole dimension of the designed lens is 300 mm × 300 mm, and its total thickness is 13 mm. In the design of the metasurface-based lens, the phase distribution can be achieved based on the reciprocity of EM wave. Here, we apply a CP patch antenna working at 3.77 GHz as the feed. In Fig. 5(a), it is seen that the metasurface-based lens is placed at a height of 40 mm above the patch antenna as the

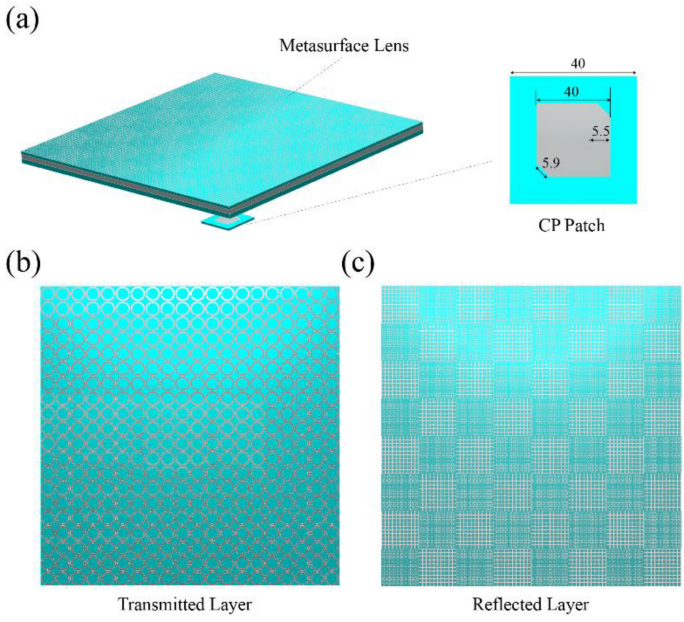

Fig. 5. (a) The view of the proposed metasurface-based lens antenna. (b) The structure patterns of the reflected layer and (c) the transmitted layer.

superstrate, and the inset shows the geometry parameters of the patch antenna. The substrate for the patch antenna is F4B with a thickness of 2 mm. Fig. 5(b) illustrates that the transmission layer is discretized into 20 $\times$ 20 phase cells, and the phase compensation is completed by the ingenious design of each phase cell. To realize a good scattering cancellation performance in the reflection mode, two types of the square loop with anti-reflection phase difference are employed to construct the whole reflection layer. As illustrated in Fig. 5c, there are 8 $\times$ 8 super units placed in a chessboard distribution, and each of the super units consists of 10 $\times$ 10 square loops. When light impinges onto such lens surface, the backward scattering field is split into four main beams as expected.

Figs. 6(a) and 6(b) reveal the gain of the metasurface-based lens antenna and the conventional patch antenna. Generally, the traditional patch antenna generates the sphere wavefront, and the apparent phase lag is observed at its two sides. When introducing the metasurface-based lens above the patch antenna, its radiation wavefront should be altered as expected. Indeed, there appears a quasi-parallel wave in the radiation area of the metasurface-based lens. Consequently, the gain-enhancement of the patch antenna could be expected through the phase modulation of the metasurface-based lens. The 3D scattering pattern of the proposed lens antenna under the normal incidence is displayed in Fig. 6(c), and Fig. 6(d) reveals that the result of a PEC slab with the same size as a comparison. It is seen that the backward scattering wave is strong for the PEC slab. However, the employing metasurface-based lens can effectively disperse the scattering wave into four directions at 11 GHz, and thus sharply reduce the monostatic RCS of the antenna. In addition, it needs to be noted that RCS-reduction performance can be realized under any polarizations because of the use of the symmetry geometry in the reflection layer of the lens.

Figs. 7(a) and 7(b) show the simulated gain versus frequency of the patch antenna with and without an metasurface-based lens. It is seen that the gain of the traditional RCP patch antenna is only about 7 dB. After introducing the lens to reshape the radiation beam, the antenna gain is sharply improved by about 6.4 dB and the maximum gain (LCP) reaches as high as 13.4 dB around 3.87 GHz. Compared with the working frequency of the primary CP patch antenna, the combined lens antenna has a frequency shift from 3.77 to 3.87 GHz, which is due to the coupling between the metasurface and the patch antenna source. In addition, the aperture efficiency (*AE*) of the designed

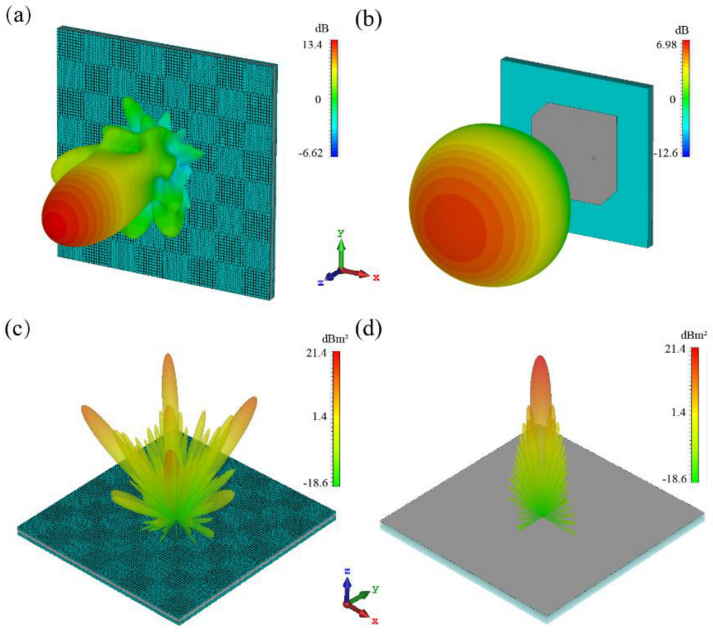

Fig. 6. (a), (b) 3D scattering patterns of the metasurface-based lens antenna and the PEC slab with the same size under normal incidence at 11 GHz. (c), (d) 3D gain of the metasurface-based lens antenna and the conventional patch antenna at 3.87 GHz.

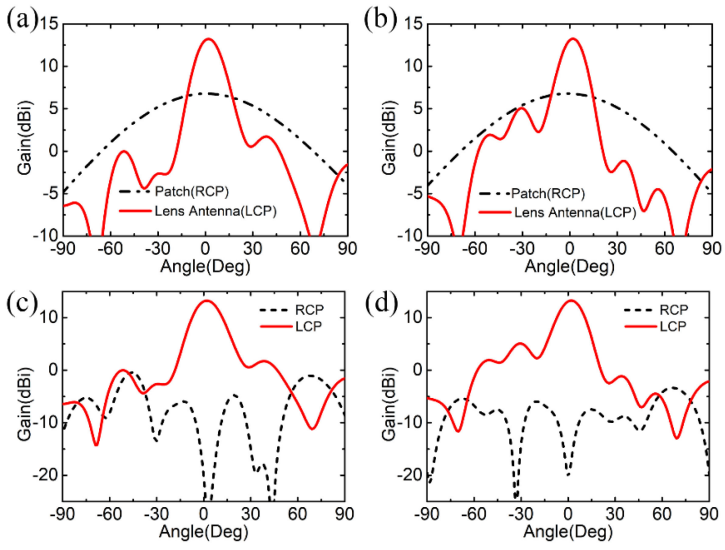

Fig. 7. Simulated gains of the patch antenna with/without the metasurface-based lens at (a) xoz-plane and (b) yoz-plane. Left-polarized and right-polarized gains of the lens antenna at xoz-plane(c) and yoz-plane(d).

metasurface lens antenna can be calculated by the following equation,

$$AE = \left(G \times \lambda^2\right) / \left(4 \times \pi \times A\right)$$

where G is the gain of the antenna, λ is the wavelength of the operate frequency, A is the geometry area of the antenna. In our design, the AE of the proposed lens antenna is 11.26%. This efficiency

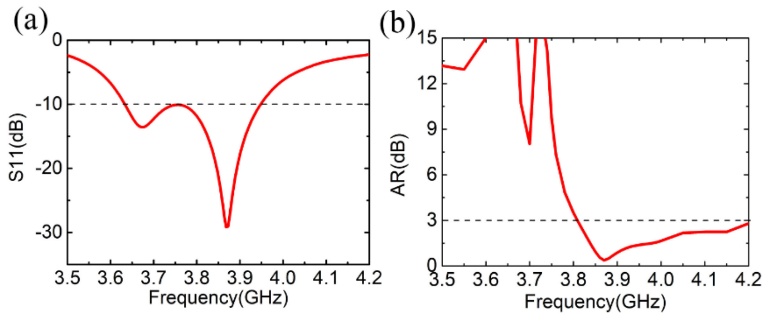

Fig. 8. Simulated S11 (a) and axial ratio (b) of the metasurface lens antenna.

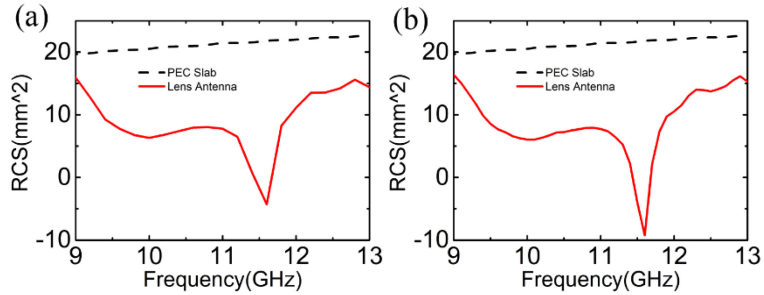

Fig. 9. Full-wave simulated RCS of the metasurface-based lens antenna and the PEC slab with the same size under normal incidence. (a) *xoz*-plane and (b) *yoz*-plane.

may be improved by further optimizing the transmissivity of the designed lens or the gain of the feeding antenna source.

Figs. 7(c) and 7(d) present the radiation patterns of the metasurface-based lens antenna in the *xoz*- and *yoz*-planes at 3.87 GHz, respectively. The directive beams are generated in both *xoz* and *yoz* planes where the isolation between RCP and LCP beams is over 30 dB. That means the proposed lens antenna has a good axial ratio (AR). The simulated reflection coefficients and AR of the metasurface-based lens antenna are respectively displayed in Figs. 8(a) and 8(b). The S11 has a −10 dB bandwidth ranges from 3.6 to 3.95 GHz. The measured 3 dB AR bandwidth is from 3.8 to 4.2 GHz, and the minimum AR that is below 0.4 occurs at 3.87 GHz, which promises a good CP wave produced by the metasurface lens.

To demonstrate the RCS reduction performance, the monostatic RCS of the proposed lens antenna under normal incidence is verified. The frequency response curves of the RCS in both *xoz* and *yoz* planes are respectively given in Figs. 9(a) and 9(b). It is obvious that the monostatic RCS of the metasurface lens antenna is dramatically suppressed over a wide frequency band due to the scattering cancellation effect of the anti-reflection phase design in the reflection layer of the lens. The 8 dB RCS reduction bandwidth is between 9 and 13 GHz, and the 10-dB bandwidth reaches from 9.2 to 12.2 GHz. A good agreement is obtained between the predicted and simulated results.

4. Conclusion

In this paper, we demonstrated a bi-functional metasurface lens antenna which can enhance the gain and reduce the RCS of the lens antenna simultaneously. The full-wave simulation results have verified that the metasurface lens not only enhances the gain of the traditional patch antenna 6.4 dB at 3.87 GHz, but also maintains the low-RCS performance from 9–13 GHz significantly. The proposed lens antenna working in full space improves the ability to manipulate the EM wave of the conventional microwave lens antenna. And the proposed metasurface also has the potentials

to design the bifunctional radome in the microwave, which may maintain the low back-scattering characteristic and reshape the beam of the antenna simultaneously.

References

[1] Y. B. Thakare and Rajkumar, "Design of fractal patch antenna for size and radar cross-section reduction," (in English), *IET Microw., Antennas Propag.*, vol. 4, no. 2, pp. 175–181, 2010.
[2] S. Simms and V. Fusco, "Thin radar absorber using artificial magnetic ground plane," *Electron. Lett*, vol. 41, no. 24, pp. 1311–1313, 2005.
[3] Z. Miao *et al.*, "Design of a patch antenna with dual-band radar cross-section reduction," *Microw. Opt. Technol. Lett.*, vol. 54, no. 11, pp. 2516–2520, 2012.
[4] H.-K. Jang, W.-J. Lee, and C.-G. Kim, "Design and fabrication of a microstrip patch antenna with a low radar cross section in the X-band," *Smart Mater. Struct.*, vol. 20, no. 1, 2010, Art. no. 015007.
[5] Y.-Q. Li, H. Zhang, Y.-Q. Fu, and N.-C. Yuan, "RCS reduction of ridged waveguide slot antenna array using EBG radar absorbing material," *IEEE Antennas Wireless Propag. Lett.*, vol. 7, pp. 473–476, 2008.
[6] S. Genovesi, F. Costa, and A. Monorchio, "Low-Profile array with reduced radar cross section by using hybrid frequency selective surfaces," *IEEE Trans. Antennas Propag.*, vol. 60, no. 5, pp. 2327–2335, May 2012.
[7] C. Huang, W. Pan, X. Ma, and X. Luo, "A frequency reconfigurable directive antenna with wideband Low-RCS property," *IEEE Trans. Antennas Propag.*, vol. 64, no. 3, pp. 1173–1178, Mar. 2016.
[8] Y. Guo, X. Ma, M. Pu, X. Li, Z. Zhao, and X. Luo, "High-efficiency and wide-angle beam steering based on catenary optical fields in ultrathin metalens," *Adv. Opt. Mater.*, vol. 6, no. 19, 2018, Art. no. 1800592.
[9] D. R. Smith, J. B. Pendry, and M. C. K. Wiltshire, "Metamaterials and negative refractive index," *Science*, vol. 305, no. 5685, pp. 788–792, 2004.
[10] V. M. Shalaev, "Optical negative-index metamaterials," *Nature Photon.*, vol. 1, no. 1, pp. 41–48, 2007.
[11] N. I. Zheludev and Y. S. Kivshar, "From metamaterials to metadevices," *Nature Mater.*, vol. 11, no. 11, pp. 917–924, 2012.
[12] X. Chen, H. F. Ma, X. Y. Zou, W. X. Jiang, and T. J. Cui, "Three-dimensional broadband and high-directivity lens antenna made of metamaterials," *J. Appl. Phys.*, vol. 110, no. 4, 2011, Art. no. 044904.
[13] T. Driscoll *et al.*, "Free-space microwave focusing by a negative-index gradient lens," *Appl. Phys. Lett.*, vol. 88, no. 8, 2006, Art. no. 081101.
[14] J. P. Turpin, W. Qi, D. H. Werner, B. Martin, M. Bray, and E. Lier, "Low cost and broadband Dual-Polarization metamaterial lens for directivity enhancement," *IEEE Trans. Antennas Propag.*, vol. 60, no. 12, pp. 5717–5726, Dec. 2012.
[15] N. Yu and Z. Gaburro, "Light propagation with phase discontinuities: Generalized laws of reflection and refraction," *Science*, vol. 334, no. 6054, pp. 333–337, 2011.
[16] N. Yu, P. Genevet, F. Aieta, and M. A. Kats, "Flat optics: Controlling wavefronts with optical antenna metasurfaces," *IEEE J. Sel. Topics Quantum Electron.*, vol. 19, no. 3, May/Jun. 2013, Art. no. 4700423.
[17] L. Zhang, S. Mei, K. Huang, and C. W. Qiu, "Advances in full control of electromagnetic waves with metasurfaces," *Adv. Opt. Mater.*, vol. 4, no. 6, pp. 818–833, Mar. 2016.
[18] H.-H. Hsiao, C. H. Chu, and D. P. Tsai, "Fundamentals and applications of metasurfaces," *Small Methods*, vol. 1, no. 4, Jun. 2017, Art. no. 1600064.
[19] X. Luo, "Subwavelength optical engineering with metasurface waves," *Adv. Opt. Mater.*, vol. 6, 2018, Art. no. 1701201.
[20] M. Pu *et al.*, "Catenary optics for achromatic generation of perfect optical angular momentum," *Sci. Adv.*, vol. 1, no. 9, 2015, Art. no. e1500396.
[21] J. Yang, C. Huang, X. Wu, B. Sun, and X. Luo, "Dual-wavelength carpet cloak using ultrathin metasurface," *Adv. Opt. Mater.*, vol. 6, no. 14, Mar. 2018, Art. no. 1800073.
[22] H. Zhu, S. W. Cheung, and T. I. Yuk, "Enhancing antenna boresight gain using a small metasurface lens: Reduction in half-power beamwidth," *IEEE Antennas Propag. Mag.*, vol. 58, no. 1, pp. 35–44, Feb. 2016.
[23] H. Barba Molina and J. Hesselbarth, "Microwave dielectric stepped-index flat lens antenna," *Int. J. Microw. Wireless Technol.*, vol. 9, no. 05, pp. 1103–1109, 2016.
[24] R. H. Phillion and M. Okoniewski, "Lenses for circular polarization using planar arrays of rotated passive elements," *IEEE Trans. Antennas Propag.*, vol. 59, no. 4, pp. 1217–1227, Apr. 2011.
[25] T. Cai, G. Wang, X. Fu, J. Liang, and Y. Zhuang, "High-efficiency metasurface with polarization-dependent transmission and reflection properties for both reflectarray and transmitarray," *IEEE Trans. Antennas Propag.*, vol. 66, no. 6, pp. 3219–3224, Jun. 2018.
[26] A. H. Abdelrahman, A. Z. Elsherbeni, and Y. Fan, "High-gain and broadband transmitarray antenna using triple-layer spiral dipole elements," *IEEE Antennas Wireless Propag. Lett.*, vol. 13, pp. 1288–1291, 2014.
[27] E. Erfani, M. Niroo-Jazi, and S. Tatu, "A high-gain broadband gradient refractive index metasurface lens antenna," *IEEE Trans. Antennas Propag.*, vol. 64, no. 5, pp. 1968–1973, May 2016.
[28] T. Cai, G. Wang, J. Liang, Y. Zhuang, and T. Li, "High-performance transmissive meta-surface for C-/X-band lens antenna application," *IEEE Trans. Antennas Propag.*, vol. 65, no. 7, pp. 3598–3606, Jul. 2017.
[29] Y. Huang *et al.*, "Catenary electromagnetics for ultra-broadband lightweight absorbers and large-scale flat antennas," *Adv. Sci.*, vol. 6, 2019, Art. no. 1801691.
[30] W. Min, H. Cheng, C. Po, W. Yanqing, Z. Zeyu, and L. Xiangang, "Controlling beamwidth of antenna using frequency selective surface superstrate," *IEEE Antennas Wireless Propag. Lett.*, vol. 13, pp. 213–216, 2014.
[31] X. Wan, X. Shen, Y. Luo, and T. J. Cui, "Planar bifunctional Luneburg-fisheye lens made of an anisotropic," *Laser Photon. Rev.*, vol. 8, no. 5, pp. 757–765, 2015.

[32] Y. Zhuang, G. Wang, T. Cai, and Q. Zhang, "Design of bifunctional based on independent control of transmission and reflection," *Opt. Express*, vol. 26, no. 3, pp. 3594–3603, 2018.
[33] J. Yang, X. Wu, J. Song, C. Huang, Y. Huang, and X. Luo, "Cascaded for simultaneous control of transmission and reflection, " *Opt. Express*, vol. 27, no. 6, pp. 9061–9070, 2019.
[34] X. Ding *et al.*, "Ultrathin Pancharatnam-Berry metasurface with maximal cross-polarization efficiency," *Adv. Mater.*, vol. 27, no. 7, pp. 1195–1200, 2015.
[35] T. J. Cui, M. Q. Qi, X. Wan, J. Zhao, and Q. Cheng, "Coding metamaterials, digital metamaterials and programmable metamaterials," *Lightw., Sci. Appl.*, vol. 3, no. 10, 2014, Art. no. e218.
[36] X. Xie *et al.*, "Plasmonic metasurfaces for simultaneous thermal infrared invisibility and holographic illusion," *Adv. Funct. Mater.*, vol. 28, no. 14, 2018, Art. no. 1706673.